Supplementary Material

MRI distortions

Susceptibility distortion

The use of a low-bandwidth FLASH pulse sequence for imaging amplifies pixel shift distortions arising from inhomogeneous magnetic susceptibility across tissue, air, and formalin compared to high-bandwidth scans (Jezzard and Balaban, 1995; Fischl et al., 2004). To test the magnitude of these geometric distortions, successive scans were acquired with positive and negative read-out directions, which, for pulse sequences employing RF excitations after data from each line of *k*-space is acquired, result in pixel displacements in opposite directions which cancel on average.

The qualitative effects of susceptibility distortions are shown in Figure S1(A) as the difference between contours of the stria drawn in the same slice of two separate acquisitions with opposite read-out direction polarities. To quantitatively evaluate the magnitude of the susceptibility distortion, the distance between the two contours was calculated at each vertex of the positive read-out contour. Figure S1(B) shows a close-up view of the outlined region of Figure S1(A). The mean distance from a vertex on the positive read-out contour to the nearest point on the negative read-out contour is 0.36 ± 0.22 mm. Since pixel shifts are in the opposite direction for the two contours, the distance between the veridical contour and a shifted one is half the distance between two oppositely shifted contours. Therefore, the average pixel shift in the region of the stria of Gennari due to susceptibility inhomogeneity is about 0.18 mm, or one voxel. It is important to note that this method underestimates the actual distortion, since calculation of the distance between contours via the closest point assumes that pixel shifts are always normal to the contours. This is not the case in general, as discussed below.

Gradient nonlinearity distortion

Another MRI distortion that affects the measured geometry of the V1 surface is geometric distortion due to the deviations from linearity of the magnetic field gradient produced by the gradient coil system. To investigate the magnitude of this type of distortion, gradient nonlinearity correction (Jovicich et al., 2006) using the three-dimensional gradient field spatial distribution specific to the coil (as supplied by the manufacturer) was applied to the same volume used to investigate susceptibility inhomogeneity distortion. The result of the gradient nonlinearity unwarping process is a vector field of displacements representing the artifactual pixel shifts due to gradient nonlinearity distortion. The coordinates of each vertex on the positive read-out contour were displaced using the gradient unwarping vector field, resulting in the unwarped contour shown in Figure S1(A).

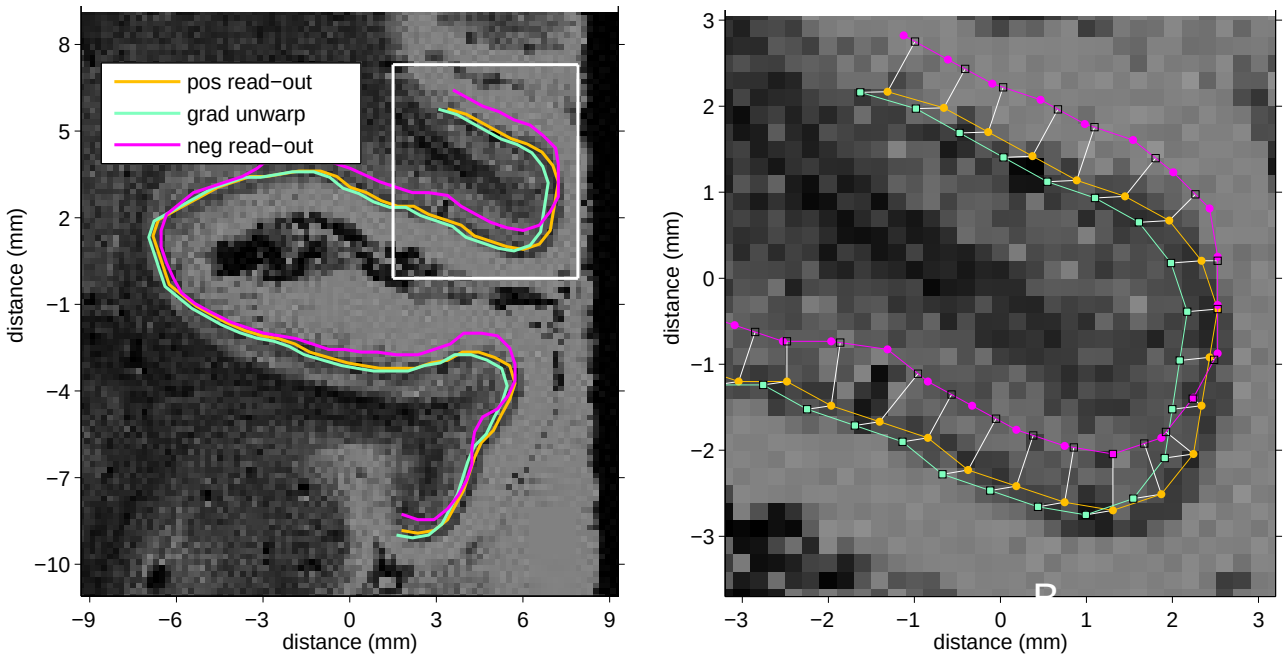

Figure S1: Examination of the MRI distortions with the largest effect on the images of the stria of Gennari. (A) A slice from a single, unaveraged volume from sample LH3. The orange curve is a contour of the stria of Gennari traced in this slice, which was acquired with a positive read-out direction polarity. The green curve shows the same contour after gradient nonlinearity distortion correction has been applied to the coordinates of the vertices in the positive read-out contour. The magenta curve is a contour traced from the stria of Gennari in the same slice as shown here, but from a volume acquired with a negative readout direction polarity, and therefore opposite pixel shifts due to susceptibility inhomogeneity. (B) A close-up view of the area delimited by the white box in (A). The different methods for computing distance between the positive and negative read-out polarity contours and the positive read-out and gradient unwarped contours are shown by the white lines, which indicate the distance between the contours (see text).

The mean displacement of the vertices in the positive read-out contour after unwarping is 0.26 ± 0.06 mm, or about 1.5 voxels. This is 50% greater than the susceptibility inhomogeneity distortion. The effect of susceptibility inhomogeneity distortion in Figure S1(A) appears by eye to be greater than gradient nonlinearity since the negative read-out contour actually represents twice the distance shift of the actual distortion, and since the method used to calculate the displacement underestimates the distance between the positive read-out and negative read-out contours. This is a result of the different methods for computing the distance between contours for the two types of distortion. In computing gradient nonlinearity distortion magnitude, the distance between corresponding vertices on the two contours can be compared directly, since the gradient unwarping provides vertex correspondence. However, a vertex in the negative read-out contour has no corresponding vertex in the positive read-out contour, so the shortest distance between the two contours is used. This method underestimates the actual distance between contours.

Distortion correction requires warping and resampling of the original MRI data. The interpolation involved in this process smooths the data, which is undesirable when working with high-resolution images. Since we determined the effects of the MRI distortions to be smaller than the features of interest in these scans, we did not apply corrections to the data presented.

Surface area estimation

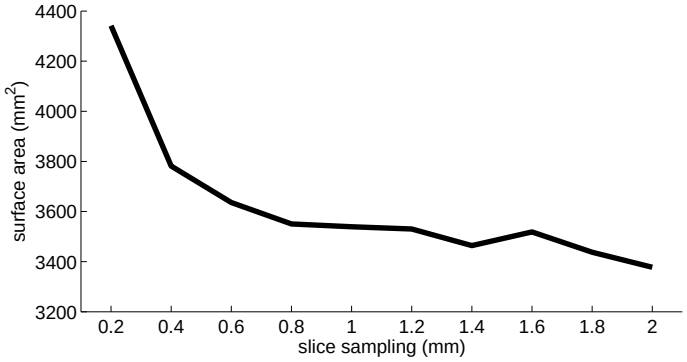

Figure S2: The total surface area of mesh reconstructions of V1 of subject RH1 as the slice sampling distance is increased from 0.2 mm to 2 mm.

When the interslice distance was small, the human tracing error present in each slice caused numerous small-scale geometric errors in the surface mesh that appear as corrugations. These errors can lead to an overestimate of the surface-based distance between vertices on different slices. In addition, we found that a there was a substantial overestimate of the surface area of V1 when the slice distance used for reconstruction was too small, as shown in Figure S2. Although the error in slice coordinates due to contour tracing has zero

mean, the distance and surface area error is strictly positive if the topology of the surface is accurate, so these small-scale geometric errors increase the observed distances and surface area. As the slice distance rises from 0.2 mm, the surface area estimate quickly asymptotes, but then starts to decrease as errors are introduced by insufficient sampling. By inspecting the agreement between the reconstructed surface mesh and the stria in the sagittal and horizontal planes, an interslice distance of 0.8 mm was determined to be appropriate for accurate surface reconstruction.

Average flattening distortion and surface curvature

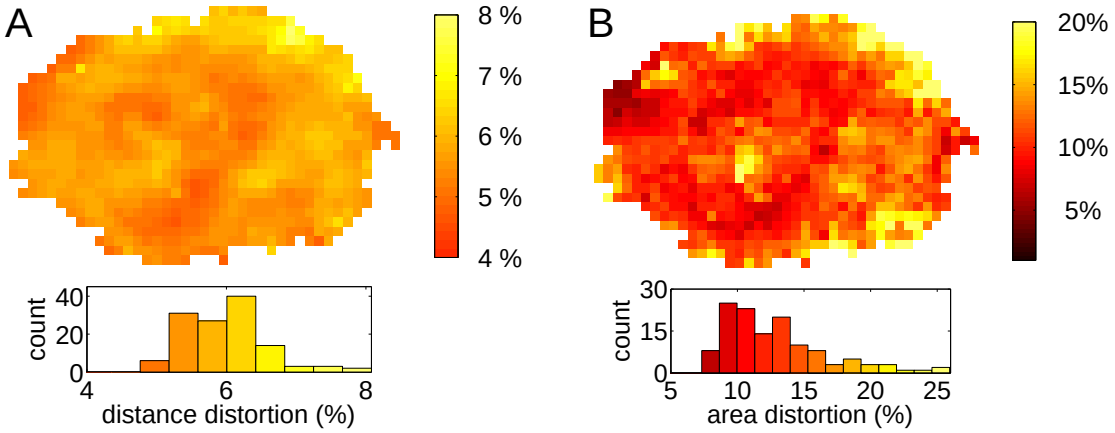

Figure S3: (A) The average distance distortion of the registered surfaces. (B) The average area distortion. In these plots anterior is to the left and dorsal is to the top.

To examine the spatial characteristics of distortions introduced by near-isometric flattening, the average flattening error was computed in the registered space. After registration, the per-vertex distance distortion for each entire flattened surface was binned, then the individual distance distortion maps were pooled and normalized. Any bins for which all flattened surfaces were not represented were excluded to avoid biasing the average error maps toward individual surfaces near the border of the map. The boundary of V1 on the flattened surfaces was ignored during computation of average error maps. The resulting spatial profile of average distance distortion resulting from the flattening process for all V1 surfaces after registration is shown in Figure S3(A). The average distance distortion in V1 was 5.6% with a 0.4% standard deviation. The relatively uniform profile of the distance distortion confirms that, in addition to the low average distance distortion for individual surfaces, the distance distortion across samples is spatially uncorrelated.

Figure S3(B) shows the spatial profile of the average area distortion in flattening, computed in the same way as the distance distortion map. The area distortion is higher than the distance distortion since distance

distortion is explicitly minimized during the flattening process. In addition, the area error exhibits more spatial correlation than the distance distortion does. The average area distortion was 11.5% with a 3.3% standard deviation.

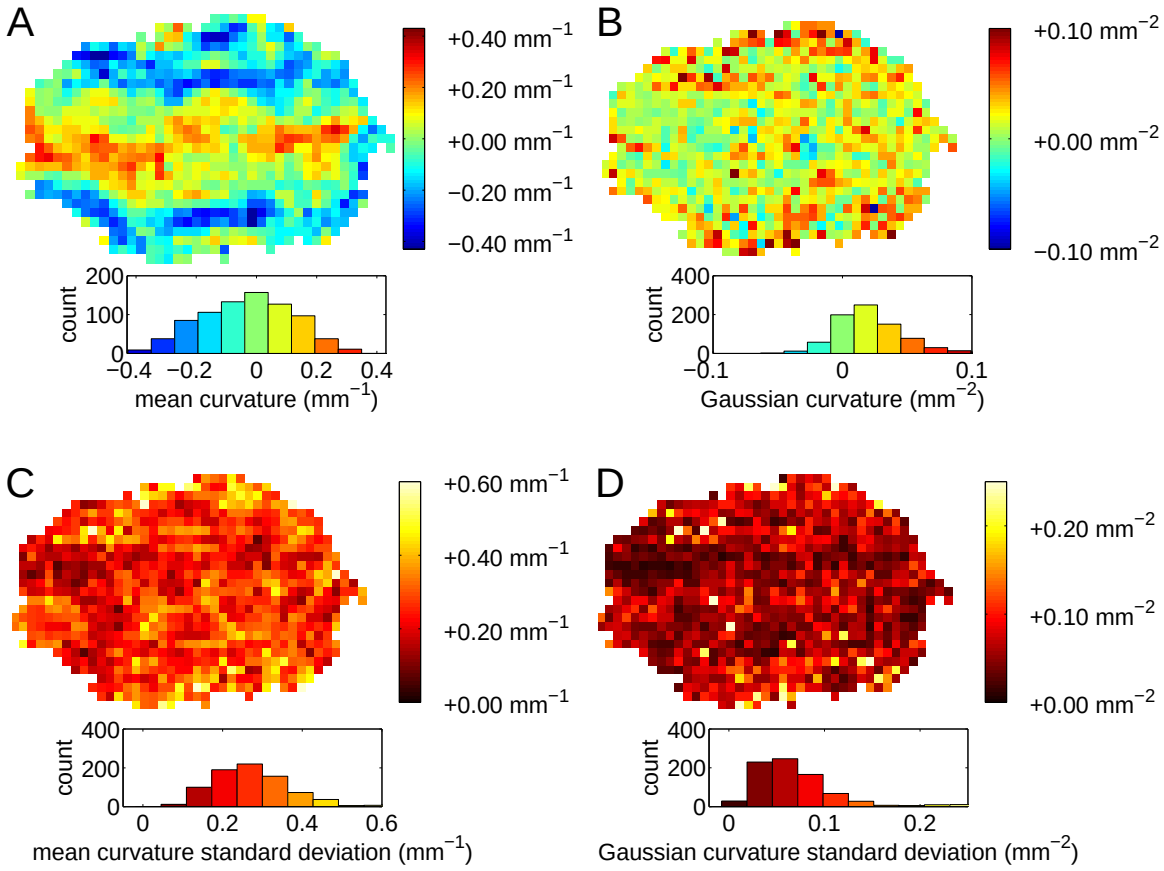

Figure S4: (A) The average mean curvature of the registered surfaces. (B) The average Gaussian curvature. (C) The standard deviation of the average mean curvature map shown in (A). (D) The standard deviation of the average Gaussian curvature map shown in (B).

To examine regularity in the curvature pattern of the cortical sheet within V1, the mean and Gaussian curvature profiles for each sample were compared. Curvature was computed by fitting a quadratic patch to each vertex and its two-ring, then computing the mean and Gaussian curvature of the surface at the vertex via the coefficients of the quadratic patch (Do Carmo, 1976). The average spatial maps in the registered space were computed in the same way as the flattening error maps, as described above.

The average mean curvature map after registration is shown in Figure S4(A). The strip of positive mean curvature parallel to the long axis of V1 shows the relative consistency of the fundus of the calcarine sulcus in relation to V1. The average Gaussian curvature map after registration, shown in Figure S4(B), exhibits a relatively uniform pattern.

The mean curvature map exhibits higher absolute values near the fundus and lips of the calcarine sulcus.

However, high curvature cannot be reliably used to predict the location of the calcarine sulcus because the variance of the mean curvature map is high (0.3 ± 0.1 mm^{-1}) compared to the average curvature, as shown in Figure S4(C).

References

Do Carmo MP. 1976. *Differential Geometry of Curves and Surfaces.* Prentice-Hall, NJ.

Fischl B, Salat DH, van der Kouwe AJ, Makris N, Segonne F, Quinn BT, and Dale AM. 2004. Sequence-independent segmentation of magnetic resonance images. NeuroImage. 23:S69–S84.

Jezzard P and Balaban RS. 1995. Correction for geometric distortion in echo planar images from B0 field variations. Magn Reson Med. 34:65–73.

Jovicich J, Czanner S, Greve D, Haley E, van der Kouwe A, Gollub R, Kennedy D, Schmitt F, Brown G, Macfall J, Fischl B, and Dale A. 2006. Reliability in multi-site structural MRI studies: effects of gradient non-linearity correction on phantom and human data. NeuroImage. 30:436–443.